Warm and moist atmospheric flow caused a record minimum July sea ice extent of the Arctic in 2020

Yu Liang[1,2,3,4], Haibo Bi[1,2,3], Haijun Huang[1,4], Ruibo Lei[5], Xi Liang[6], Bin Cheng[7], Yunhe Wang[1,2,3]

[1] Key Laboratory of Marine Geology and Environment, Institute of Oceanology, Chinese Academy of Sciences, Qingdao,
266071, China

[2] Laboratory for Marine Geology, Qingdao National Laboratory for Marine Science and Technology, Qingdao, 266061, China

[3] Center for Ocean Mega-Science, Chinese Academy of Sciences, Qingdao, 266071, China

[4] University of Chinese Academy of Sciences, Yuquan Road 19, Beijing 100049, China

[5] Key Laboratory for Polar Science of the State Oceanic Administration, Polar Research Institute of China, Shanghai 200136,
China

[6] Key Laboratory of Research on Marine Hazard Forecasting Center, National Marine Environmental Forecasting Center,
Beijing, 100081, China

[7] Polar Meteorology and Climatology, Finnish Meteorological Institute, Helsinki, PO Box 33 FIN-00931, Finland

Correspondence to: Haijun Huang (hjhuang@qdio.ac.cn)

Abstract. The satellite observations unveiled that the July sea ice extent of the Arctic shrank to the lowest value in 2020 since 1979, with a major ice retreat in the Eurasian shelf seas including Kara, Laptev, and East Siberian Seas. Based on the ERA-5 reanalysis products, we explored the impacts of warm and moist air-mass transport on this extreme event. The results reveal that anomalously high energy and moisture converged into these regions in the spring months (April to June) of 2020, leading to a burst of high moisture content and warming within the atmospheric column. The convergence is accompanied by local enhanced downward longwave radiation and turbulent fluxes, which is favorable for initiating an early melt onset in the areas with severe ice loss. Once the melt begins, solar radiation played a decisive role in leading to further sea ice depletion due to ice-albedo positive feedback. The typical trajectories of the synoptic cyclones that occurred on the Eurasian side in spring 2020 agree well with the path of atmospheric flow. Assessments suggest that variations in characteristics of the spring cyclones are conducive to the severe melt of sea ice. We argue that large-scale atmospheric circulation and synoptic cyclones act in concert to trigger the exceptional poleward transport of total energy and moisture from April to June to cause this new record minimum of sea ice extent in the following July.

1 Introduction

Arctic sea ice is declining dramatically (Wang et al., 2019) under the background of global warming (Hinzman et al., 2005; Comiso and Hall, 2014; Johannessen et al., 2016) and Arctic Amplification (Screen and Simmonds, 2010; Serreze and Barry, 2011; Kim et al., 2016). Sea ice extent (SIE) minima of the Arctic reached its record low in September 2012 over all the

satellite observations during the period 1979-2020, stood at 3.40×10^6 km^2. After that, 2020 witnessed the second-lowest September SIE in the Arctic, which ended up only 3.74×10^6 km^2. During the seasonal cycle of the sea ice cover in 2020, SIE grew to its maximum on March 5, then decreased persistently in the following warm months. Roughly speaking, Arctic sea ice cover turned to be smaller in extent during spring and early summer than that of 2012. Consequently, in 2020, Arctic sea ice

35   experienced the lowest July extent recorded since 1979. As estimated, the July SIE of 2020 shrunk to 7.01×10^6 km^2, which is ~8% (or ~21%) lower than that of 2012 (or the average July SIE over the period 2000-2020). Figure 1 demonstrates the spatial pattern of sea ice concentration (SIC) anomalies and the corresponding SIE in July 2020. During the early summer of 2020, a prominent SIC reduction occurred in the Eurasian shelf seas, including Kara, Laptev, and East Siberian Seas (60° E-165° E and 70° N-82° N, as represented by green polygon in Fig. 3c and d, hereafter the study area). The averaged SIC anomaly in

40   these areas of 2020 (-25.96%) exceeds corresponding anomalies from all other years during the period 1979-2020. Therefore, the sea ice retreat in these regions contributed remarkably to the distinguished shrinkage of SIE in the Arctic Ocean in July 2020.

The severe retreat of Arctic sea ice provides vital implications of environmental change, and it could have a diverse impact on regional and even global climate (Overland et al., 2015; Gu et al., 2018; Previdi et al., 2020), marine ecology (Post et al.,

45   2013), economic activities (Crépin et al., 2017). Likewise, the scientific studies about the causes of Arctic sea ice shrinkage encompass various disciplines. Regarding the sea ice-atmosphere interactions, previous studies provided a consensus that changes in both large-scale atmospheric circulation (Wu et al., 2006; Deser and Teng, 2008; Hegyi and Taylor, 2018; Lei et al., 2019) and synoptic activities (e.g., cyclones) (Zhang et al., 2013a; Olason and Notz, 2015; Lei et al., 2016; Wernli and Papritz, 2018; Lei et al., 2020) could significantly impact sea ice variation. Atmospheric forcing plays an important role in regulating

50   the sea ice variations and trends through both thermodynamic and dynamic processes. With respect to the thermodynamics, the heat and moisture advection from mid-latitudes increase the air temperature, humidity, and cloudiness, thereby altering the surface radiation and energy budget in the Arctic (Doyle et al., 2011; Graversen et al., 2011; Zhang et al., 2013a; Boisvert et al., 2016; Dufour et al., 2016; Vázquez et al., 2017). Dynamically, wind anomalies can induce sea ice motion and deformation, leading to sea ice redistribution and the occurrence of cracks, leads, and polynyas (Brümmer et al., 2001; Vihma et al., 2012;

55   Olason and Notz, 2015; Lei et al., 2020; Liang et al., 2021).

At present, the new record low Arctic sea ice extent (SIE) in July 2020, especially in the study area, has not garnered much attention. The underlying mechanisms contributing to this extreme event remain unclear. Inspired by the previous works, we conduct an assessment for the preconditions in meteorological fields during the spring months just prior to the record minimum SIE in July 2020. Specifically, we examine the magnitude and variations of the atmospheric transport of total

60   energy and moisture as well as their convergence over the Arctic in spring (April-June) 2020. The changes in terms of the temperature and specific humidity fields over the vast area with significant sea ice retreat due to the convergence of the energy and water vapor are explored. To quantify the sea ice melt due to changes in the surface energy balance, the energy flux

components including downward longwave radiation, solar radiation, and turbulent fluxes are analyzed. Moreover, we

investigate the distinct role of the synoptic activities, which contributes to the remarkable anomalies of the moisture and

65   energy fluxes into the area of substantial ice loss.
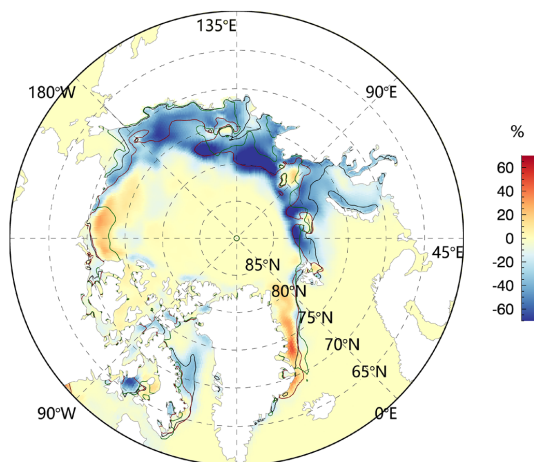
Figure 1. Spatial patterns of SIC anomalies (shading), and the SIEs in typical years (bold lines). The red line represents the SIE in July 2020. Green and grey curves within denote the SIE in July 2012 and the 20-yr average of the recent period 2001-2020, respectively. The anomalies are computed as the difference between the fields in July and the corresponding climatology over the past four decades (1979-2020).

70   **2 Data and methods**

2.1 Data

We use the Polar Pathfinder Daily sea ice motion (SIM) vectors product and satellite-derived daily sea ice concentration (SIC)

provided by the National Snow and Ice Data Center (NSIDC) to investigate the SIE variations over the ice-retreated area. The

SIM product is derived from a variety of sensors on satellite platforms, merged with buoy observations as well as reanalyzed

75   wind data. The motion data is georeferenced to the Equal-Area Scalable Earth (EASE) Grids. The upgrade of the most recent

SIM (Version 4.0) addresses artifacts resulting from interpolation (Tschudi et al., 2019). Tschudi et al. (2019) show that the

NSIDC SIM product is one of the most comprehensive sea ice motion datasets. SIC fields are available on a polar

stereographic projection and are derived from the SMMR, the SSM/I, and the SSMIS by applying the bootstrap algorithm

(Comiso, 2017). The latest version (Version 3.1) of the dataset provides improved consistency between sensors through the use

80   of a suite of daily varying tie points generated from the AMSR-E observations. Both datasets have a spatial resolution of 25 km

and a temporal resolution of 1-day.

     We use daily sea ice thickness (SIT) from the Pan-Arctic Ice Ocean Modeling and Assimilation System (PIOMAS) (Zhang

and Rothrock, 2003). PIOMAS is a coupled sea-ice/ocean model which is forced by atmospheric fields and sea surface

temperatures from the National Centers for Environmental Prediction/National Center for Atmospheric Research

85 ((NCEP/NCAR) reanalysis. Multiple studies have compared PIOMAS SIT fields with satellite, submarine, airborne, and in

situ observations, whose results revealed that PIOMAS is highly consistent with these observations (Zhang and Rothrock,

2003; Schweiger et al., 2011; Stroeve et al., 2014; Wang et al., 2016). In particular, Schweiger et al. (2011) outlined a less than

0.1-m mean difference and a high pattern correlation (r = +0.8) between the PIOMAS and the ICESat-derived SIT fields. The

PIOMAS SIT dataset is available on a generalized orthogonal curvilinear coordinate system with a mean resolution of 22 km.

90   Cryosphere Science Research Portal (CSRP) of National Aeronautics and Space Administration (NASA) provides the

record of sea ice surface melt dates in the Arctic, wherein the knowledge concerning the onset of the melt season is obtained.

The fields are derived from SSM/I data following Markus et al. (2009) and available on the data grid in line with the SIC

fields provided by NSIDC.

         ERA5 reanalysis datasets including sea level pressure (SLP), temperature, specific humidity, surface evaporation, wind

95 speed, the vertical integral of northward/eastward water vapor flux, the vertical integral of northward/eastward total energy

flux and their convergence, as well as the radiation parameters (surface net/downward longwave radiation, surface

net/downward shortwave radiation, surface latent heat flux and surface sensible heat flux) are obtained from the European

Centre for Medium-Range Weather Forecasts (ECMWF). These meteorological variables are used to identify cyclones and

extract the associated characteristic variables (track, intensity, center, et al.), and to quantify the atmospheric energy and

100 moisture transport. Previously, Kapsch et al. (2013) found ERA-Interim to be the most credible reanalysis for the Arctic

climate. ERA5 is a new reanalysis product that benefits from a decade of developments in model physics, core dynamics, and

data assimilation, replacing the ERA-Interim. Compared with ERA-Interim, the major strength of ERA5 is the much higher

temporal and spatial resolutions than those of previous global reanalyses and better performance in the troposphere (Hersbach

et al., 2020). The adopted ERA5 datasets are characterized by a spatial resolution of 1.0° ×1.0° in longitude and latitude. Note

105 that most of the ERA5 variables we utilized are recorded every six hours except for parameters that accumulated over a

particular time period (evaporation and surface radiation fluxes) and the convergence of the energy and moisture transport.

2.2 Methods

2.2.1 The atmospheric transport of total energy and moisture

The net atmospheric moisture transport for the Arctic represents regionally integrated precipitation minus evapotranspiration

110 and the precipitable water tendency. However, large errors and sparse uncertainties exist in precipitation and

evapotranspiration measurements (Zhang et al., 2013b). To this end, we utilize wind and specific humidity fields from

reanalysis, which are of great fidelity, to compute moisture transport. The vertical integral of northward moisture flux can be

approximated following the trapezoidal rule (Dufour et al., 2016):

$$\int_0^{p_s} f(p)dp \approx \sum_{n=n_0}^{N-1} \frac{1}{2}[f(p_{n+1}) + f(p_n)](p_n - p_{n+1})$$
$$+ f(p_{n_0})(p_s - p_{n_0}) \tag{1}$$

115     $f(p_n) = v_n q_n$ (2)

where n is the number of pressure levels, n_0 is the lowest pressure level. p_n corresponds to pressure at the nth pressure level,

v_n and q_n represents the northward component of the wind speed and specific humidity at the nth pressure level, respectively.

We compared our estimated results of the vertical integrated northward water vapor flux against the existing dataset archived

in ERA5. The results (not shown) show that the estimated results are highly consistent with the corresponding ERA5 filed

120   both in the magnitude and change of all months across various latitudes (e.g., 70° N) during the period 1979 to 2020, which

lends credence to the direct use of the water vapor flux field obtained from ERA5. By the same token, we take advantage of

the vertical integral of total energy from ERA5. The vertically integrated, atmospheric, northward energy transport consists of

internal, potential, kinetic and latent energy.

2.2.2 Changes in sea ice thickness due to melt

125   Changes in surface energy budget related to energy and water vapor convergence affect sea-ice melting. The thickness of melt

caused by alteration of surface energy budget can be calculated via the sea-ice growth model (Maykut et al., 1992; Eisenman et

al., 2007). Neglecting some smaller radiative fluxes, the changes in sea ice thickness can be written as a simplified function of

the surface radiation and turbulent flux:

$$-\Delta h = \frac{\Delta t}{\rho L}[FL_{w\downarrow} + FS_{w\downarrow} + H_\downarrow + LE_\downarrow] \tag{3}$$

130   where Δh represents sea-ice change, Δt is the time step, ρ represents the density of sea ice (917 kg/m³), L is the latent

heat of fusion for sea ice (333.4 kJ/kg), $FL_{w\downarrow}$ and $FS_{w\downarrow}$ represent the surface net fluxes of longwave and shortwave

radiation, respectively. $H_\downarrow$ corresponds to the sensible heat, and $LE_\downarrow$ denotes the latent heat.

2.2.3 Cyclone identification and tracking

To examine the effects of cyclone activities on the anomalous energy and moisture transport in spring 2020, we use a revised

135   automatic cyclone identification and tracking algorithm developed originally by Serreze et al. (1993) to diagnose the center

positions and trajectories of the cyclones from the 6-hourly SLP data (Serreze et al., 1993; Serreze, 1994; Serreze et al., 1997;

Wang et al., 2006; Wang et al., 2013). The cyclone detection and tracking algorithm consists of two steps: (1) Inspecting the

candidate center where the pressure is lower by 0.1 hPa than the surrounding grid points (Wang et al., 2013). If multiple

cyclone center candidates are found within a radius of 1200 km, the one with the largest local Laplacian of SLP is determined

140   as the exact cyclone center. (2) Tracking the centers between two consecutive time steps based on the "nearest neighbor" rule

to form trajectories, with further checks including the distance moved in specific directions and pressure tendency. Therefore,

a cyclone track consists of a series of cyclone centers identified in sequential time steps at adjacent locations. In this study,

thresholds related to multiple parameters, including the maximum travel distance (800 km), maximum north-, south- and west-ward migration (600 km), and maximum pressure tendency (20 hPa) (Serreze, 1994; Wang et al., 2006), are adopted.

145   Note that regions with surface elevations higher than 1000 m are excluded since the algorithm tends to detect spurious systems due to larger uncertainty in the SLP over mountainous terrain.

Moreover, the corresponding features for each cyclone, including the duration, intensity, and radius, were also retrieved. By definition, the intensity is referred to as the difference between the SLP of the cyclone center and the climatological monthly mean SLP at corresponding grid points. The density of tracks denotes the number of distinct cyclones occurring in a

150   particular region during spring. We use an integrative parameter to measure the intensity, number, and duration of a cyclone. The Cyclone Activity Index (CAI) is defined as the sum of the intensity over all cyclone centers in a particular region during the spring months (Zhang et al., 2004). A more detailed description of the automated cyclone detection and tracking scheme can be found in Liang et al. (2021).

3 Atmospheric energy and moisture transport

155   The transport of total energy and moisture toward the Arctic system is controlled by changes in large-scale atmospheric circulation and patterns of climatic variability (Graversen et al., 2011; Vihma et al., 2016; Ding et al., 2017). As depicted in Fig. 2, the average Arctic atmospheric condition from April to June 2020 was dominated by a persistent low-pressure anomaly centered over the north pole and extended southwards from the Barents-Kara Seas to the middle part of northern Eurasia. Two high-pressure anomaly centers were located in Eastern Siberia and around the Norwegian Sea, respectively. These SLP modes

160   favor anomalous southerly winds, which transport moist and warm air mass from Eurasia into the Arctic through the entry in the Kara Sea. After entering the Arctic Ocean, the air mass was deflected to move along the coast of Eurasia and influenced the shelf seas.
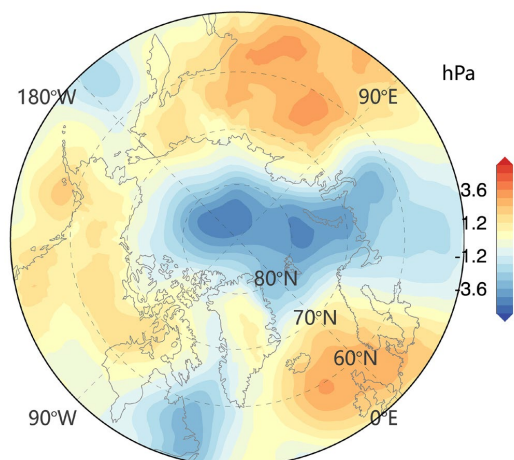
Figure 2. Spatial patterns of SLP anomalies (shading) during April to June 2020. The anomalies are computed as the difference between the
165   averaged fields of the three months (April-June) and the corresponding climatology over the past four decades (1979-2020).

Using ERA5 reanalysis, we quantify the anomalies of the vertical integral of meridional total energy and water vapor flux.

As shown in Fig. 3, an anomalously large advection of energy and water vapor from lower latitudes, which is diverted by wind

variations, prevailed in the region with conspicuous sea ice retreat (Fig. 1) in spring 2020. Regions around the Laptev and Kara

sea (45° E-120° E, 70° N) are the main entry channels for warm air-mass input from lower latitudes. It is estimated that the

170   zonal mean of the meridional total energy flux (water vapor flux) through these main entry channels over the entire spring in

2020 reached up to 1.74×10^{11} Wm^{-1} (1.51×10^3 kg m^{-1}s^{-1}), producing a transport that was 2 (3) standard deviations larger than

the 1979-2020 climatology. The pronounced poleward energy and moisture through the entry then converged into the Arctic.

As depicted in Fig. 3c and d, the major parts of the ice-retreated shelf seas in spring 2020 are characterized by positive

convergence anomalies of the atmospheric moisture and energy transport. Particularly, the magnitude of the total energy and

175   moisture flux convergence anomaly even exceeds 50 Wm^{-2} and 9×10^{-6} kg m^{-1}s^{-2}, respectively, in the Kara Sea).
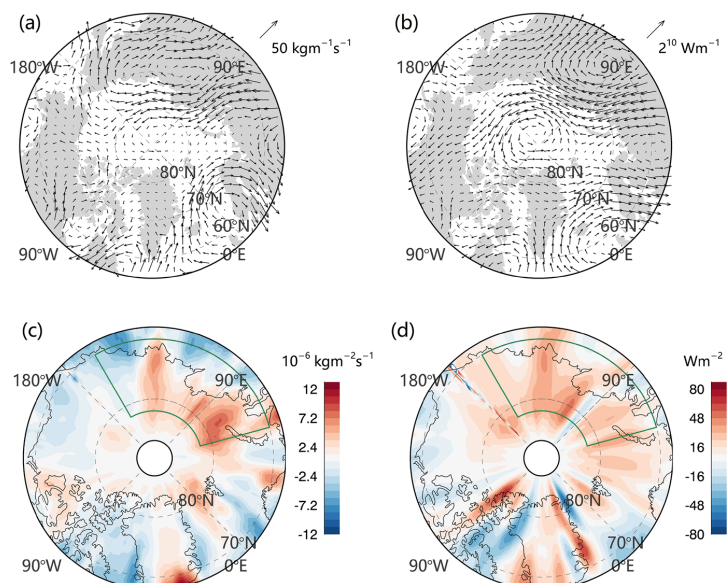
Figure 3. Anomalies of the vertically integrated northward (a) moisture flux and (b) total energy transport and the corresponding convergence (c-d) averaged over the spring months (April-June) of 2020. Anomalies are relative to the climatology of April-June from the years 1979-2020. Green polygons encapsulate areas where substantial sea ice cover loss (60° E-165° E, 70° N-82° N) occurred in July 2020, which represents the study area of this paper.

Figure 4 illustrates the meridional cross-sections of temperature and specific humidity anomalies spanning the regions with maximum convergence of the atmospheric fluxes (60° E-165° E, 60° N -90° N). Horizontally, elevated temperature and higher moisture content distributed widely from 60° N to 85° N near the surface. Vertically, the positive temperature and moisture anomalies extend conspicuously into the mid-troposphere (~750 hPa). The intrusion of moisture and energy leads to surface warming (damping) of up to 3-4 K ($6-8\times10^{-4}$ kg kg^{-1}) in the spring months. The vertical patterns of the anomalies indicate that the great convergence (Fig. 3c and d) of energy and moisture could contribute to the local increases in the atmospheric temperature and humidity, both at the surface and in the troposphere above the boundary layer, which is in agreement with the finding of Graversen et al. (2008). Noticeably, unusual conditions that higher moisture content and warming within the Arctic atmospheric column prevailed over the ice cover loss region. We also examine the role of local evaporation in the regional increase of moisture under a warmer Arctic climate. According to the ERA5 reanalysis, the spring evaporation over the Arctic Basin exhibits a decreasing trend over the past four decades, except for the Barents and Norwegian Seas. In April-June 2020, below-normal evaporation dominated the Arctic with an averaged negative value of -1.5×10^{-4} m in the regions with notable ice-retreat (not shown). The decline in evaporation indicates that the enhanced moisture contributing to the moister atmosphere over these regions is primarily provided by atmospheric transport from remote areas rather than by local sources as the moisture fluxes from the sea surface are negligible. This finding further affirms the

arguments of Vázquez et al. (2016) and Singh et al. (2017), which highlighted the importance of remote sources of water vapor.
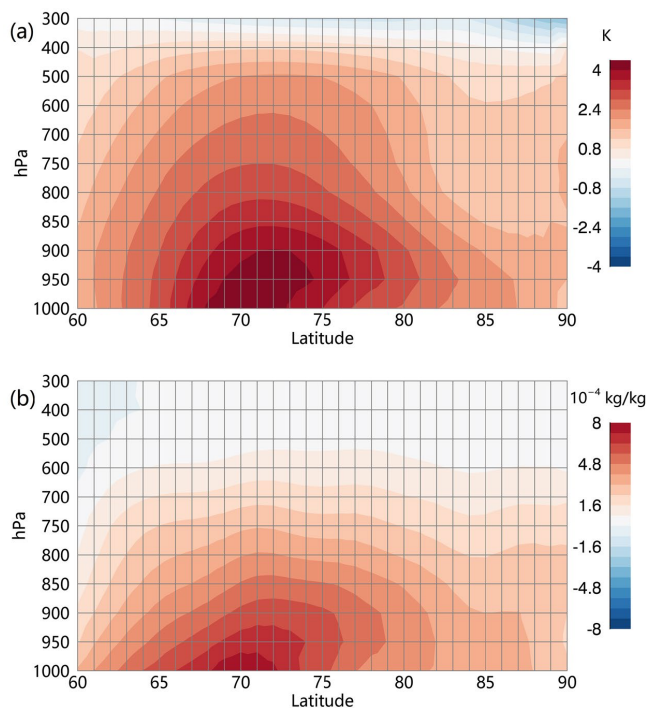
Figure 4. Vertical cross-sections of zonal averaged (a) air temperature and (b) specific humidity anomalies, as a function of latitude and pressure level, during the spring months (April–June) of 2020 spanning the with significant energy and moisture convergence (60° E-165° E, 60° N-90° N). The anomalies are calculated as the difference between the averaged fields of the three months (April-June) and the corresponding climatology over the past four decades (1979-2020).

4 Surface energy Budget

The surface energy budget that consists of thermal radiation, solar radiation, and turbulent fluxes is vital for sea ice melt and growth. An increase of humidity associated with the convergence of moisture flux may strengthen cloud formation(Johansson et al., 2017), of which both contribute to the enhanced local greenhouse effect. In addition, the energy convergence in the atmosphere may partly be radiated directly to space in the form of longwave radiation, and partly radiated to the sea surface and turbulently mixed, contributing to the sea ice melt. Having shown the anomalously large convergence of water vapor and total energy transport in April-June 2020, in the following we will present the variations of different surface energy flux components. Note that the ECMWF convention for vertical fluxes is positive downwards.

In the Eurasian shelf seas with remarkable sea ice shrinkage, the surface gained more energy owing to both shortwave and longwave radiation, as well as turbulent fluxes, as the enhanced surface fluxes predominantly appeared in these regions (Fig. 5). The spatial pattern of anomalies in surface thermal radiation downwards is characterized by positive values throughout the

convergence zones, with the largest amplitudes in the Kara Sea (~32 Wm^{-2}, Fig. 5a). The anomalies of the net longwave

215 radiation (Fig. 5b) are roughly similar in spatial distribution to that of the downward component over the Arctic marginal seas

on the Eurasian side. The difference between Fig.5a and b indicates that part of thermal radiation was radiated upwards to

increase the surface air temperature before the melt commenced. Downward and net shortwave radiation anomalies are

portrayed in Fig. 5d and e. The downward component of the solar radiation was below-normal in most parts of the ice-retreated

area (Fig. 5d), which is presumably attributed to increased cloudiness associated with the convergence of moisture. In contrast,

220 remarkably positive anomalies of the net solar radiation were found in the Eurasian shelf seas where the extensive loss of sea

ice is observed. This is a result of the substantial formation of open water due to sea ice loss which reduces the albedo and

thereby enables the upper ocean to absorb more heat (i.e., the ice-albedo feedback).

Additionally, sensible and latent turbulent surface flux anomalies both make a contribution to the energy surplus at the

surface in the spring months of 2020 (Fig. 5c and f). The positive (downward) anomalies of turbulent surface fluxes were

225 detected in the regions which coincide well with the seas with contracted ice cover (Fig. 5c and f). Intuitively, more turbulent

fluxes would be released to the atmosphere as more open water prevailed. That is, a negative (upward) value over the Arctic

shelf seas is expected. However, reduced upward, or even downward, sensible and latent heat fluxes are detected in the study

region during April-June in 2020. This can be attributed to the anomalously high moisture advection and convergence which

as a result could reduce the gradient of the water vapor pressure at the surface. As implied in Fig.4, positive temperature and

230 humidity anomalies extend from surface even to mid-troposphere, peaks at around 925 hPa. These changes would result in a

decreased vertical gradient in air temperature and humidity in the lower atmosphere, reducing the hypothesized upward

turbulent fluxes from the ocean surface to the overlying atmosphere.
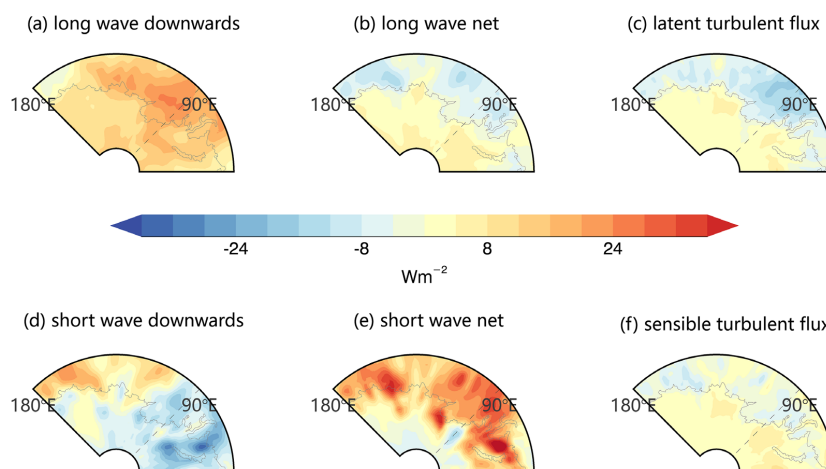
Figure 5. Anomalies of surface (a) downwelling and (b) net longwave radiation, (d) downwelling and (e) net shortwave radiation, as well as
235 sensible (c) and latent (f) heat fluxes. The anomalies are relative to the climatology with monthly resolution from the years 1979-2020 and
averaged over the spring months (April–June) of 2020.

Figure 6a presents the time series of SIE, the anomalies of atmospheric energy transport convergence and the surface fluxes averaged over the study area (enclosed by the green polygon in Fig. 3c and d) during 2020. Indeed, the energy convergence event started at the end of March and lasted for three months, peaked in early June. This is followed by an augment in the

240   downward thermal radiation plus turbulent fluxes (smaller) by ~30-40 Wm^{-2} (Fig. 6a, green line). The almost simultaneous response of downward thermal radiation highlights that the convergence of the total energy and moisture flux has a significant imprint on the increased surface energy fluxes. With the enhanced downward infrared radiation, sea ice cover began to decrease gradually (Fig. 6a, grey line). The time development underlines that the positive anomalies of longwave radiation plus turbulent fluxes played a significant role in initiating an early than usual melt in 2020. As estimated from fields of melt

245   dates archived in NASA, persistent melt conditions in the study area were observed in May 2020 (Fig. 6, red vertical line), which occurred about 15 days earlier than the average value of the period 1979-2020. As the melt commenced, the formation of open water decreased the surface albedo, which in turn acted to increase the absorption of solar radiation (Fig. 6a, red line). That is, the earlier melt onset could foster stronger ice-albedo feedback(Hall, 2004), leading to an accelerated decline in SIE in June-July when the anomaly of net solar radiation reached its maximum.

250
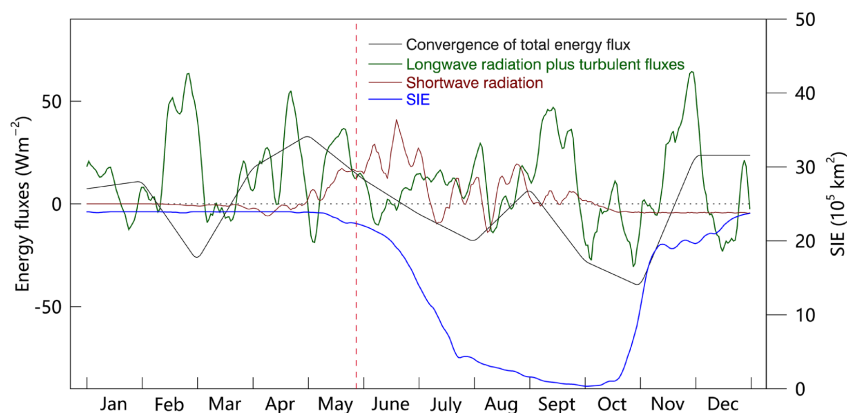
Figure 6. Time series of SIE, the anomalies of atmospheric energy transport convergence and surface energy fluxes over the study area (indicated by the green polygon in Fig. 3c and d) during 2020. The blue curve represents the SIE. The red line denotes the anomalies of net solar radiation. The green line corresponds to the anomalies of the sum of the downwelling thermal radiation and the turbulent (latent plus sensible) flux. The vertical pink line denotes the average melt day (May 28) in 2020, provided by NASA. The anomalies are relative to the

255   climatology of the years 1979-2020.

To quantify the thermodynamic impact of atmospheric energy of spring 2020 on the sea ice melt, we calculate the changes in sea-ice thickness due to the variations of surface energy fluxes via the sea-ice growth model(Maykut et al., 1992; Eisenman et al., 2007). According to equation (3), a 1 W/m^{-2} increase in surface energy budget during three spring months (April to June) would melt approximately 2.60 cm of sea ice. The spatial pattern of sea ice thickness change due to surface energy

260   fluxes variations, calculated by equation (4), is portrayed in Fig. 7a. SIT anomalies due to radiative forcing are mostly negative (i.e., melting) in the Kara, Laptev, and East Siberian Seas during the three spring months of 2020, with a particularly

large value (-1.2m) in the Kara sea (Fig.7a). The region with significant SIT reduction agrees well with that with distinct SIC anomalies.

265   To reiterate the long-term changes, we examine the trend of SIT over the past four decades in the study area. As estimated from the thickness data provided by PIOMAS, the average thickness of spring (April-June) sea ice in the study area has a remarkable decreasing trend of -0.27 m per decade (significant at the 99% confidence level) in the past four decades (Fig. 7b). SIT was persistently lower than 2.50 m since 2000 and dropped sharply to only 1.20 m in the spring of 2020. Thinner ice is more susceptible to changes thermodynamically forcing, thus prone to melt earlier, which in turn could foster a stronger summer ice-albedo feedback through the formation of open water areas. In other words, without the extensive

270   coverage of thin, first-year ice in spring 2020 in the study area (Fig. 7b), the unusual atmospheric energy and moisture transport would not have been nearly as effective in reducing ice extent as was observed (Fig. 1).
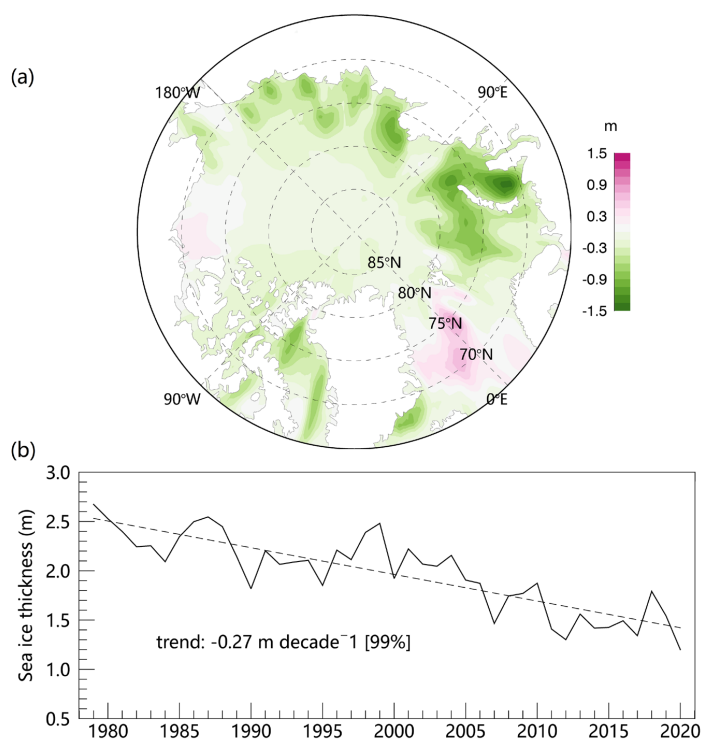
Figure 7. (a) Changes of SIT caused by anomalies of surface radiative fluxes during spring (April-June) 2020 which is estimated by a sea-ice growth model. (b) Time series of SIT (provided by PIOMAS) and the corresponding trend (dashed line) averaged over the study area (60° E-165° E and 70° N-82° N) in spring during the period 1979-2020.

275

5 Cyclones activities in Spring 2020

Synoptic cyclones are a central component maintaining the global atmospheric energy, moist, and momentum budgets(Jakobson and Vihma, 2010; Dufour et al., 2016; Villamil-Otero et al., 2018). A wide variety of studies reveal a

poleward shift in tracks and significant changes in the frequency and intensity of extratropical cyclones(Yin, 2005; Sepp and

280 Jaagus, 2011; Zhang et al., 2013a; Day et al., 2018). Considering the notable variations in cyclone activities and the strong sea

ice decline experienced in the study area over recent decades, understanding the underlying effects of the cyclones on the

poleward transport of energy/moisture is especially crucial. We identify and tracking cyclone systems that occurred in the

spring months (April - June) during the period 1979-2020 using the automated algorithm(Serreze et al., 1993; Serreze, 1994;

Serreze et al., 1997; Wang et al., 2006; Wang et al., 2013). To cross-check the cyclone systems diagnosed from the ERA5 SLP,

285 we also analyzed data from ERA-interim. Despite some differences in certain regions, a high agreement exists in terms of

interannual variability and climatological geographical distribution of cyclone characteristics (not shown). To some extent,

this consistency gives credence to the method and datasets utilized.

Longitudinal distributions of the climatological vertically integrated northward total energy and moisture flux across 60° N,

as well as CAI of cyclones entering the Arctic at the 60° N averaged over the spring months (April–June) during 1979-2020,

290 are illustrated in Fig. 8. Note that cyclones entering the Arctic are defined as cyclone trajectories having their cyclolysis south

of 60° N and traveling poleward through 60° N. The spatial distribution of CAI is in good agreement with the vertically

integrated meridional total energy and moisture flux. The main entry channels of the energy and moisture including the North

Atlantic, North Pacific, and the Labrador Seas witness more cyclones with greater intensity that propagated toward the Arctic

region. A strong correlation exists between the averaged CAI and the vertically integrated northward total energy flux

295 (moisture flux) at 60° N with R=+0.69 (+0.68) (361 grids, significant at the 99% confidence level), suggesting the significant

role of cyclone activity in contributing to the poleward advection of energy and moisture. Note that Greenland is masked when

tracking cyclones to avoid problems caused by SLP extrapolation, hence we use the latitude 60° N other than 70° N to display

the relationship between cyclone activities and the meridional fluxes. Other studies also corroborated the fact that synoptic

cyclones play a crucial role in regulating the poleward fluxes considering the fundamental nature of cyclones in holding and

300 transporting moisture and energy. For instance, Dufour et al. (2016) concluded that poleward advection of moisture is

dominated by transient eddies (e.g., cyclones) owing to its almost exclusively meridional direction of the flux. It was estimated

that the cyclones could explain 80–90% of the total northward transport at latitudes of 70° N(Jakobson and Vihma, 2010;

Dufour et al., 2016). In addition, Villamil-Otero et al. (2018) found that stronger cyclone activity across 60° N measured by the

CAI generally co-occurs with enhanced poleward monthly atmospheric moisture transport in each representative seasonal

305 month. Our results augment evidence for the view that the intrusion of moisture and energy associated with cyclones into the

Arctic is linked with the abrupt changes in the Arctic climate system.
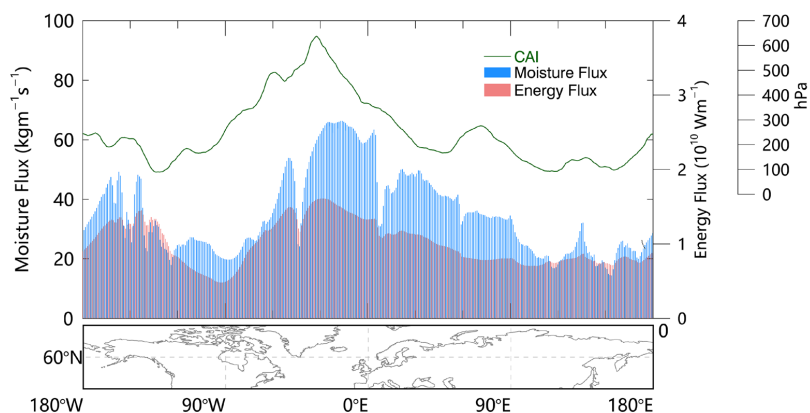
Figure 8. Longitudinal distributions of the climatological vertically integrated meridional total energy and moisture flux across 60° N, as well as CAI of cyclones entering the Arctic at the 60° N averaged over the spring months (April–June) during 1979-2020.

310   It is noteworthy that, in this study, we use a range of latitudes (50° N-70° N, with a step length of 1°), other than a single

one, to define the poleward cyclones. For instance, poleward cyclones are defined as those that are generated south of a certain

latitude within the range (50° N-70° N) and traveling northward through it. All of these cyclones may play a non-negligible

role in carrying energy and water vapor to the Arctic in the form of a relay. As shown in Fig. 9, spring 2020 saw many

low-pressure systems moving poleward from Eurasia and some of them entered the study area through the main entry channels

315   in the Kara sea (Fig. 9, green thin lines). Besides, in the Eurasian shelf seas with great convergence of the total energy and

water vapor transport (Fig. 3c and d), the majority of the cyclones are featured with trajectories in a zonal direction (Fig. 9,

blue thin lines). Furthermore, we retrieve the typical trajectory paths of these cyclones following Gaffney (2004). The

trajectory clustering was done using a polynomial regression mixture model where each cyclone trajectory is approximated as

a second-order polynomial. The detected cyclones during the spring months (April-June) of 2020 are clustered in two

320   categories, which are schematically explained in Fig. 9 with thick polylines. One track represents the cyclones that are

generated in the lower latitude of Eurasia with a poleward moving tendency, while the other denotes cyclones in the marginal

seas that are characterized by an eastward movement toward or through the Kara, Laptev, and East Siberian Seas (Fig. 9). In

general, the trajectories of these cyclones as observed during the spring months (April-June) of 2020 coincide well with the

path of total energy and water vapor transport (Fig. 3a and b). The good agreement implies that these extratropical cyclones in

325   spring, as shown in Fig. 9, served as a vital carrier of the anomalously large amount of energy and moisture into the study

area. To sum up, the synoptic cyclones act in concert with the large-scale atmospheric circulation to cause anomalous energy

and moisture fluxes into the study area and to change the characteristics of the Arctic climate system.
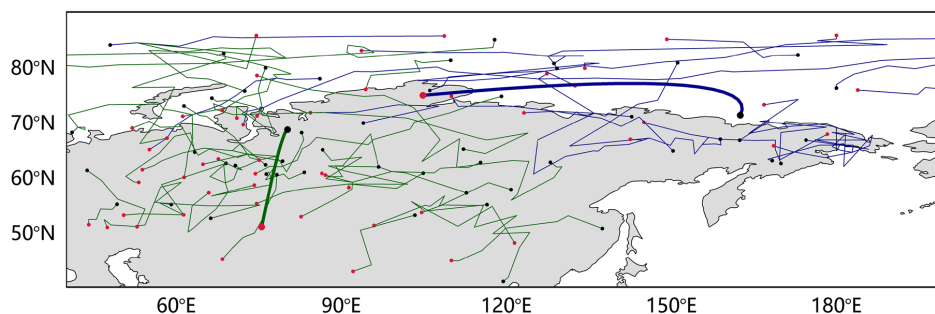
Figure 9. Poleward cyclones detected in the main entry channels (green thin line, 45° E-120° E and 40° N-90° N) and all cyclones occurred in the regions intersected with the route after the fluxes entering Arctic (blue thin line, 45° E-15° W and 65° N-90° N) during the spring months (April-June) in 2020 and their typical trajectories (thick lines). Red (black) dots represent the position of the genesis (lysis) of cyclones.

We further investigate the connection between the long-term changes in poleward cyclones and meridional transport. Figures 10a illustrates the decadal relationship between the 10-year running trends that have been observed in the meridional total energy/moist transport and the poleward cyclone activities in spring (April-June) during the period 1979-2020. Note that the northward transport is the average value of all the corresponding fluxes across 50° N-70° N, which is consistent with the definition of poleward cyclones. Indeed, a robust correlation exists between the trends of the average intensity of poleward cyclones and the vertical integral of northward energy (moisture) transport during spring with a strong correlation coefficient of +0.62 (+0.59), suggesting poleward cyclone activities play an important role in regulating the variations of the decadal trends in meridional transport of energy and moisture. Particularly, in the recent decade (2010-2020), significant upward trends are observed in the northward transport of total energy and moisture together with more intense poleward cyclones (Fig. 10a). As for the spring months of 2020, stronger and more frequent cyclones are detected in the Arctic (Fig. 10b and c). The density of cyclone tracks is higher than normal in many parts of marginal seas and the central Arctic Ocean, with the largest positive values centered over the Taymir Peninsula. Most cyclones throughout the Arctic Basin have unusually high intensity than the climatology of the years 1979-2020, especially in the Barents, Kara, Laptev, and Beaufort Seas, indicating lower-than-normal SLP in these regions (Fig. 10c). The spatial pattern of CAI anomalies is roughly in line with those of track density and intensity (Fig. 10d).
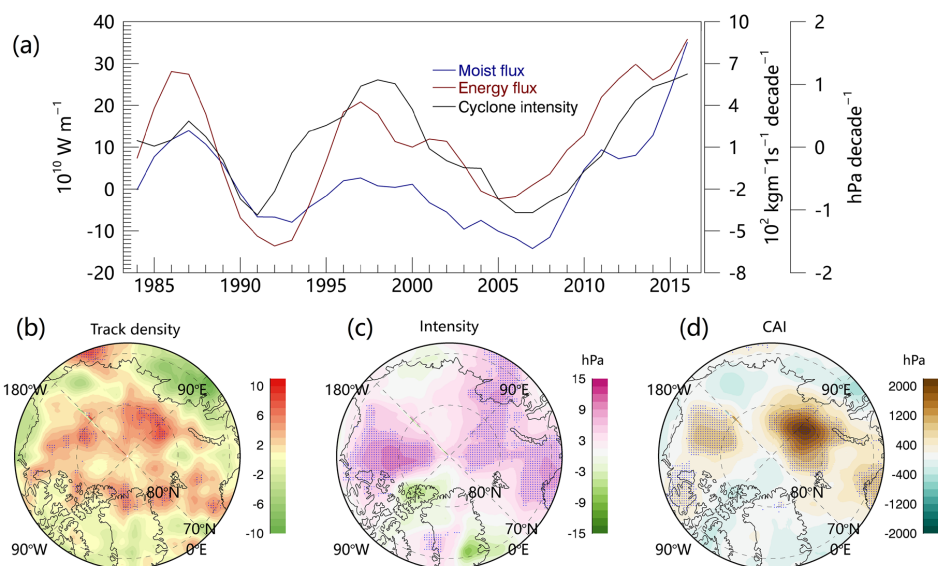
Figure 10. (a) The time series for the trends of the meridional total energy (moisture) transport and average intensity of poleward cyclone during spring months (April to June) from 1979 to 2020. The trends are calculated using a 10-year running window. Note that the northward transport is the average value of all the corresponding fluxes across 50° N-70° N, which is consistent with the definition of poleward cyclones. Anomalies of the cyclone features in spring 2020 relative to the climatology of the years 1979-2020, including the (b) density of tracks, (c) intensity, and (d) CAI. Panels (a) have units of counts per $10^6 \, km^2$ while (b) and (c) have units of hPa per $10^6 \, km^2$. Blue dots represent the regions with values above the mean plus 1.5 above standard deviation.

In general, the Eurasian shelf seas had more frequent and stronger cyclones in the spring, especially in the Kara and Laptev seas (Fig. 10). The cyclone variations could alter the spatiotemporal characteristics of the critical near-surface atmospheric parameters (wind stress, temperature, and humidity). As a result, the atmospheric conditions could have a significant impact on sea ice in the study area through control on ice motion, deformation, and melt associated with both dynamic and thermodynamic processes of a cyclone.

From the thermodynamical view, the enhancement of the total energy and water vapor transport in the Eurasia side (Fig. 3a and b) is associated with the regional increases both in the number (Fig. 10b) and intensity (Fig. 10c) of synoptic cyclones that occurred in the main entry channels and some part of the study area. The warm and moist air mass carried by cyclones in spring (Fig. 9) could alter the surface energy balance, thus initiating the earlier melt onset of sea ice as observed in the study area. Moreover, the cyclones traversing the Arctic can trigger a spatially extensive sea ice melting with their associated frontal systems(Stramler et al., 2011). The cyclones and the associated frontal systems can also affect the formation of low-level and midlevel clouds over the Arctic Ocean(Curry et al., 1996). All these thermodynamic factors may contribute to the significant SIT decline in Eurasia shelf seas as shown in Fig. 7. Dynamically, the extreme loss of SIE in July 2020 was accompanied by a strong pattern of anomalous cyclonic SIM in spring (Fig.11), with Ekman drift out of the central Arctic toward the marginal seas. On one hand, the cyclonic SIM anomaly in cold seasons serves to enhance the production of new ice within leads

370   because of the increase in sea ice divergence. On the other hand, as the melt season commences, while ice divergence increases

extent, it can also accelerate melt by exposing more dark open water areas in the cracks, leads, and polynyas. More frequent

and intense cyclones in the Arctic during spring 2020 (Fig. 10) may provide additional cyclonic wind anomalies which are

superimposed on that of the large-scale atmospheric circulation as depicted in Fig. 2, promoting the above processes. Based on

our results, the thermodynamical other than dynamical effects of cyclones seem to play a dominant role in regulating the

375   changes in SIE during spring 2020, as the expansion of sea ice cover due to divergence was offset by the significant shrinkage

due to melt.
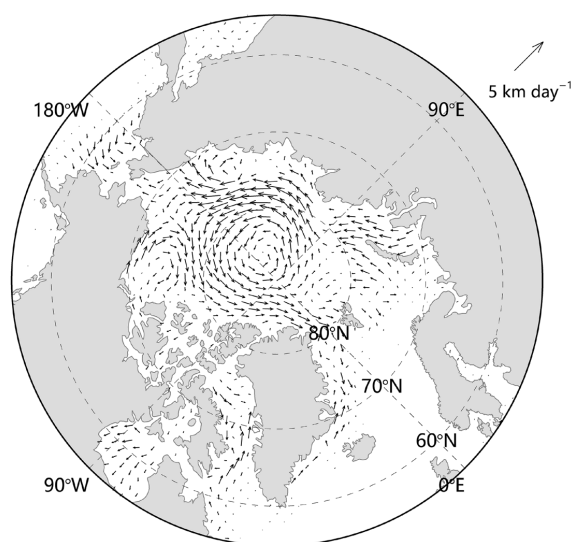
Figure 11. Anomalies of the spring (April to June) SIM relative to the climatology of the years 1979-2020.

6   Discussion and Conclusions

380   An unprecedented reduction in SIE was observed in July 2020 since the satellite era (1979-2020), especially in the Eurasia

shelf seas covering the Kara, Laptev, and East Siberian Seas (60° E-165° E, 70° N-82° N). By utilizing global reanalysis

datasets and satellite observations, we address the mechanisms of the extreme event. The variations of the total energy and

moisture transport toward the study area are obtained and analyzed. We investigate the associated surface energy budget

during spring (April to June) of 2020 to disentangle the driving effects of different energy components on sea ice in July.

385   Moreover, the influences of large-scale atmospheric circulation and synoptic cyclones on the poleward energy and moisture

transport are outlined.

Our results reveal that anomalously high advection of energy and water vapor prevailed during spring (April-June) 2020

over the regions where conspicuous sea ice retreat occurred in the following July. The enhanced energy and moist transport

converged into the study area through the main entry channels in the Laptev and Kara Seas from lower latitudes, which

390   reached up to 1.74×10^{11} Wm^{-1} and 1.51×10^{3} kg m^{-1}s^{-1} respectively, over the entire spring. As a consequence, the convergence

of the transport increased the temperature and specific humidity of the local atmosphere from the surface to the

middle-troposphere. This is accompanied by a strengthened downward longwave radiation plus turbulent fluxes at the surface,

which initiated the earlier melt onset of sea ice in the study area (15 days in advance). After the melt commenced, the enhanced

net solar radiation absorbed by dark water due to ice-albedo feedback produced an accelerated decline in SIE. Quantitative

395   analysis shows that the amount of surface radiative fluxes surplus (~40 Wm^{-2}) during April–June 2020 in the ice-retreat

domain can potentially melt around 1 meter of ice in addition to the climatological melt. Besides, having experienced a large

reduction in thickness during recent decades (-0.27 m per decade), the majority of the present sea ice in the study area is

composed of thinner seasonal ice(Kwok, 2018). We conclude that the fact of younger and thinner sea ice, together with

enhanced total energy and moisture transport which affect the surface radiative forcing, having repercussions for the

400   occurrence of the record low July SIE in 2020.

A key driver of the anomalous high transport of the total energy and moisture during spring 2020 was a persistent

atmospheric pattern, featuring unusually low SLP over the north pole which extended through the Barents-Kara Sea to Eurasia

and unusually high-pressure centers over the Eastern Siberia and the Norwegian Sea. The SLP pattern led to southerly winds

and favored the enhanced transport of warm and moist air mass from Eurasia to the adjacent Arctic shelf seas where

405   substantial sea ice retreat was observed in July 2020. Besides, the typical trajectories of the synoptic cyclones that occurred on

the Eurasian side in the spring months of 2020 agree well with the path of the intensive total energy and water vapor transport.

The agreement implies that cyclones served as another important carrier of the large energy and moist fluxes into the study

area since the storm is capable of holding moisture and energy. Further analysis reveals that the enhanced atmospheric fluxes

in spring may be partly attributed to the stronger and more frequent cyclone activities near the region with severe loss of SIE.

410   Moreover, anomalously frequent and intense cyclones in the Arctic during spring 2020 coupled with large-scale atmospheric

circulation, further strengthen the cyclonic wind and ice motion. The cyclonic ice drift could lead to extensive sea ice melt as

presented in July 2020 through the large formation of the cracks and leads among sea ice floes.

Likewise, previous studies have investigated the relationship between synoptic activities and sea ice variability. For

instance, Persson (2012) found that the synoptic-scale weather systems that augmented the atmospheric energy fluxes to the

415   surface can trigger the melt onset at a specific site and a certain year. Moisture transport associated with the synoptic activity

may explain part of regional differences in sea ice extent and concentration variations, such as in the Barents and Kara

Seas(Kapsch et al., 2014; Woods and Caballero, 2016). Nevertheless, the impacts of cyclones on sea ice depend on the location

of the cyclone tracks as the movement of cyclones determine the transport of heat and moisture as well as the direction of sea

ice drift ice(Thorndike and Colony, 1982; Brümmer et al., 2001; Liang et al., 2021). In the present study, we explored the

420   influence of cyclones qualitatively because of the strong coupling between the large-scale atmospheric circulation and synoptic

activities(Cohen et al., 2017; Koyama et al., 2017). Besides, the coupled interaction between sea ice and atmosphere involves

myriad physical processes which may lead to diverse and nonlinear effects on the Arctic ice, as well as triggering multiple feedback mechanisms. Disentangling their effects is challenging which requires using more sophisticated statistical techniques, combined with climate models of higher fidelity. The environment of the Arctic has transformed to a new state with

425   younger(Rigor and Wallace, 2004; Tschudi et al., 2016)and thinner(Kwok and Rothrock, 2009; Johnson et al., 2012; Bi et al., 2018) ice floes. Under such a circumstance, comprehensive and quantitative analysis of different mechanisms associated with cyclone activity would be an appropriate avenue for follow-up research. It is also noteworthy that despite the exceptionally low sea ice extent in July 2020, which is the focus of the present study, the September SIE minima did not exceed that of 2012, as the sea ice decline slowed down after late July. The mechanisms that retard the rapid sea ice melt remain unclear, other possible

430   processes like sea ice export variability, and multi-year ice cover should be explored in greater detail in future studies.

Data availability

NSIDC sea ice motion is available at https://nsidc.org/data/NSIDC-0116/versions/4. NSIDC sea ice concentration data is obtained from https://nsidc.org/data/NSIDC-0079/versions/3. Sea ice thickness from PIOMAS is downloaded from http://psc.apl.uw.edu/research/projects/arctic-sea-ice-volume-anomaly/data/model_grid. Sea ice melt dates are available at

435   https://earth.gsfc.nasa.gov/index.php/cryo/data/arctic-sea-ice-melt. The ERA5 reanalysis datasets were obtained from the website https://cds.climate.copernicus.eu/cdsapp#!/search?type=dataset.

Author contribution

YL carried out the analysis, processed the data, and wrote the manuscript. HB designed the method to calculate the moisture flux and performed experiments. YW processed the sea ice datasets. HH contributed to the ERA5 data collection. All authors

440   contributed to the discussion and provided ideas during the concept phase and the writing process.

Competing interests.

The authors declare that they have no conflict of interest.

Acknowledgments

This work was supported by the General Project of Natural Science Foundation of Shandong Province

445   (ZR2020MD100), National Natural Science Foundation of China under Grant (41406215 and 42076185), Key Deployment Project of Centre for Ocean Mega-Research of Science, Chinese Academy of Sciences (COMS2020Q12), the Open Funds for the Key Laboratory of Marine Geology and Environment, Institute of Oceanology, Chinese Academy of Sciences (MGE2020KG04)

References

450   Bi, H., Zhang, J., Wang, Y., Zhang, Z., Zhang, Y., Fu, M., Huang, H., and Xu, X.: Arctic Sea Ice Volume Changes in Terms of Age as Revealed From Satellite Observations, IEEE Journal of Selected Topics in Applied Earth Observations and Remote Sensing, 11, 2223-2237, 2018.

Boisvert, L. N., Petty, A. A., and Stroeve, J. C.: The Impact of the Extreme Winter 2015/16 Arctic Cyclone on the Barents–Kara Seas, Monthly Weather Review, 144, 4279-4287, 10.1175/mwr-d-16-0234.1, 2016.

455   Brümmer, B., Müller, G., Affeld, B., Gerdes, R., Karcher, M., and Kauker, F.: Cyclones over Fram Strait: impact on sea ice and variability, Polar Research, 20, 147-152, 10.3402/polar.v20i2.6511, 2001.

Cohen, L., Hudson, S. R., Walden, V. P., Graham, R. M., and Granskog, M. A.: Meteorological conditions in a thinner Arctic sea ice regime from winter through summer during the Norwegian Young Sea Ice expedition (N-ICE2015), Journal of Geophysical Research Atmospheres, 2017.

460   Comiso, J. C., and Hall, D. K.: Climate trends in the Arctic as observed from space, Wiley Interdisc Rev Clim Change, 5, 389-409, 10.1002/wcc.277, 2014.

Comiso, J. C.: Bootstrap Sea Ice Concentrations from Nimbus-7 SMMR and DMSP SSM/I-SSMIS, Version 3, https://doi.org/10.5067/7Q8HCCWS4I0R., 2017.

Crépin, A.-S., Karcher, M., and Gascard, J.-C.: Arctic climate change, economy and society (ACCESS): Integrated
465   perspectives, Ambio, 46, 341-354, 2017.

Curry, J. A., Schramm, J. L., Rossow, W. B., and Randall, D.: Overview of Arctic Cloud and Radiation Characteristics, Journal of Climate, 9, 1731-1764, 1996.

Day, J. J., Holland, M. M., and Hodges, K. I.: Correction to: Seasonal differences in the response of Arctic cyclones to climate change in CESM1, Climate Dynamics, 50, 3905-3907, 2018.

470   Deser, C., and Teng, H.: Evolution of Arctic sea ice concentration trends and the role of atmospheric circulation forcing, 1979-2007, Geophysical Research Letters, 35, Artn L02504
10.1029/2007gl032023, 2008.

Ding, Q., Schweiger, A., L'Heureux, M., Battisti, D. S., Po-Chedley, S., Johnson, N. C., Blanchard-Wrigglesworth, E., Harnos, K., Zhang, Q., and Eastman, R.: Influence of high-latitude atmospheric circulation changes on summertime
475   Arctic sea ice, Nature Climate Change, 7, 289-295, 2017.

Doyle, J., Lesins, G., Thackray, C., Perro, C., Nott, G., Duck, T., Damoah, R., and Drummond, J.: Water vapor intrusions into the High Arctic during winter, Geophysical research letters, 38, 2011.

Dufour, A., Zolina, O., and Gulev, S. K.: Atmospheric moisture transport to the Arctic: Assessment of reanalyses and analysis of transport components, Journal of Climate, 29, 5061-5081, 2016.

480   Eisenman, I., Untersteiner, N., and Wettlaufer, J. S.: On the reliability of simulated Arctic sea ice in global climate models, Geophysical Research Letters, 34, 265-278, 2007.

Gaffney, S.: Probabilistic curve-aligned clustering and prediction with regression mixture models, University of California, Irvine, 2004.

Graversen, R. G., Mauritsen, T., Tjernström, M., Källén, E., and Svensson, G.: Vertical structure of recent Arctic warming,
485   Nature, 451, 53-56, 2008.

Graversen, R. G., Mauritsen, T., Drijfhout, S., Tjernström, M., and Mårtensson, S.: Warm winds from the Pacific caused extensive Arctic sea-ice melt in summer 2007, Climate dynamics, 36, 2103-2112, 2011.

Gu, S., Zhang, Y., Wu, Q., and Yang, X. Q.: The linkage between Arctic sea ice and midlatitude weather: In the perspective of energy, Journal of Geophysical Research: Atmospheres, 123, 11,536-511,550, 2018.

490   Hall, A.: The role of surface albedo feedback in climate, Journal of Climate, 17, 1550-1568, 2004.

Hegyi, B. M., and Taylor, P. C.: The unprecedented 2016–2017 Arctic sea ice growth season: the crucial role of atmospheric rivers and longwave fluxes, Geophysical Research Letters, 45, 5204-5212, 2018.

Hersbach, H., Bell, B., Berrisford, P., Hirahara, S., Horányi, A., Muñoz-Sabater, J., Nicolas, J., Peubey, C., Radu, R., and Schepers, D.: The ERA5 global reanalysis, Quarterly Journal of the Royal Meteorological Society, 146, 1999-2049,
495   2020.

Hinzman, L. D., Bettez, N. D., Bolton, W. R., Chapin, F. S., Dyurgerov, M. B., Fastie, C. L., Griffith, B., Hollister, R. D., Hope, A., Huntington, H. P., Jensen, A. M., Jia, G. J., Jorgenson, T., Kane, D. L., Klein, D. R., Kofinas, G., Lynch, A. H., Lloyd, A. H., McGuire, A. D., Nelson, F. E., Oechel, W. C., Osterkamp, T. E., Racine, C. H., Romanovsky, V. E., Stone, R. S., Stow, D. A., Sturm, M., Tweedie, C. E., Vourlitis, G. L., Walker, M. D., Walker, D. A., Webber, P. J., Welker, J. M., Winker, K. S., and Yoshikawa, K.: Evidence and Implications of Recent Climate Change in Northern Alaska and Other Arctic Regions, Climatic Change, 72, 251-298, 10.1007/s10584-005-5352-2, 2005.

Jakobson, E., and Vihma, T.: Atmospheric moisture budget in the Arctic based on the ERA-40 reanalysis, International Journal of Climatology, 30, 2175-2194, 2010.

Johannessen, O. M., Bengtsson, L., Miles, M. W., Kuzmina, S. I., Semenov, V. A., Alekseev, G. V., Nagurnyi, A. P., Zakharov, V. F., Bobylev, L. P., Pettersson, L. H., Hasselmann, K., and Cattle, H. P.: Arctic climate change: observed and modelled temperature and sea-ice variability, Tellus A: Dynamic Meteorology and Oceanography, 56, 328-341, 10.3402/tellusa.v56i4.14418, 2016.

Johansson, E., Devasthale, A., Tjernström, M., Ekman, A. M., and L'Ecuyer, T.: Response of the lower troposphere to moisture intrusions into the Arctic, Geophysical Research Letters, 44, 2527-2536, 2017.

Johnson, M., Proshutinsky, A., Aksenov, Y., Nguyen, A. T., Lindsay, R., Haas, C., Zhang, J., Diansky, N., Kwok, R., and Maslowski, W.: Evaluation of Arctic sea ice thickness simulated by Arctic Ocean Model Intercomparison Project models, Journal of Geophysical Research Oceans, 117, doi:10.1029/2011JC007257, 2012.

Kapsch, M.-L., Graversen, R. G., and Tjernström, M.: Springtime atmospheric energy transport and the control of Arctic summer sea-ice extent, Nature Climate Change, 3, 744-748, 2013.

Kapsch, M. L., Graversen, R. G., Economou, T., and Tjernström, M.: The importance of spring atmospheric conditions for predictions of the Arctic summer sea ice extent, Geophysical Research Letters, 41, 5288-5296, 2014.

Kim, K.-Y., Hamlington, B. D., Na, H., and Kim, J.: Mechanism of seasonal Arctic sea ice evolution and Arctic amplification, The Cryosphere, 10, 2191-2202, 2016.

Koyama, T., Stroeve, J., Cassano, J., and Crawford, A.: Sea Ice Loss and Arctic Cyclone Activity from 1979 to 2014, Journal of Climate, 30, 4735-4754, 10.1175/jcli-d-16-0542.1, 2017.

Kwok, R., and Rothrock, D. A.: Decline in Arctic sea ice thickness from submarine and ICESat records: 1958–2008, Geophysical Research Letters, 36, 2009.

Kwok, R.: Arctic sea ice thickness, volume, and multiyear ice coverage: losses and coupled variability (1958–2018), Environ Res Lett, 13, 105005, 2018.

Lei, R., Heil, P., Wang, J., Zhang, Z., Li, Q., and Li, N.: Characterization of sea-ice kinematic in the Arctic outflow region using buoy data, Polar Research, 35, doi: 10.3402/polar.v35.22658, 2016.

Lei, R., Gui, D., Hutchings, J. K., Wang, J., and Pang, X.: Backward and forward drift trajectories of sea ice in the northwestern Arctic Ocean in response to changing atmospheric circulation, International Journal of Climatology, 2019.

Lei, R., Gui, D., Heil, P., Hutchings, J. K., and Ding, M.: Comparisons of sea ice motion and deformation, and their responses to ice conditions and cyclonic activity in the western Arctic Ocean between two summers, Cold Regions Science and Technology, 170, 102925, 2020.

Liang, Y., Bi, H., Wang, Y., Huang, H., Zhang, Z., Huang, J., and Liu, Y.: Role of Extratropical Wintertime Cyclones in Regulating the Variations of Baffin Bay Sea Ice Export, Journal of Geophysical Research: Atmospheres, 126, e2020JD033616, 2021.

Markus, T., Stroeve, J. C., and Miller, J.: Recent changes in Arctic sea ice melt onset, freezeup, and melt season length, Journal of Geophysical Research: Oceans, 114, 2009.

Maykut, G. A., Grenfell, T. C., and Weeks, W. F.: On estimating spatial and temporal variations in the properties of ice in the polar oceans, Journal of Marine Systems, 3, 41-72, 1992.

Olason, E., and Notz, D.: Drivers of variability in Arctic sea-ice drift speed, Journal of Geophysical Research Oceans, 119, 5755-5775, 2015.

Overland, J., Francis, J. A., Hall, R., Hanna, E., Kim, S.-J., and Vihma, T.: The melting Arctic and midlatitude weather

  patterns: Are they connected?, Journal of Climate, 28, 7917-7932, 2015.

Persson, P. O. G.: Onset and end of the summer melt season over sea ice: Thermal structure and surface energy perspective
545  from SHEBA, Climate dynamics, 39, 1349-1371, 2012.

Post, E., Bhatt, U. S., Bitz, C. M., Brodie, J. F., Fulton, T. L., Hebblewhite, M., Kerby, J., Kutz, S. J., Stirling, I., and Walker,
  D. A.: Ecological consequences of sea-ice decline, Science, 341, 519-524, 2013.

Previdi, M., Janoski, T. P., Chiodo, G., Smith, K. L., and Polvani, L. M.: Arctic amplification: A rapid response to radiative
  forcing, Geophysical Research Letters, 47, e2020GL089933, 2020.

550 Rigor, I. G., and Wallace, J. M.: Variations in the age of Arctic sea-ice and summer sea-ice extent, Geophysical Research
  Letters, 31, 2004.

Schweiger, A., Lindsay, R., Zhang, J., Steele, M., Stern, H., and Kwok, R.: Uncertainty in modeled Arctic sea ice volume,
  116, https://doi.org/10.1029/2011JC007084, 2011.

Screen, J. A., and Simmonds, I.: The central role of diminishing sea ice in recent Arctic temperature amplification, Nature,
555  464, 1334-1337, 2010.

Sepp, M., and Jaagus, J.: Changes in the activity and tracks of Arctic cyclones, Climatic Change, 105, 577-595,
  10.1007/s10584-010-9893-7, 2011.

Serreze, M. C., Box, J. E., Barry, R. G., and Walsh, J. E.: Characteristics of Arctic synoptic activity, 1952–1989,
  Meteorology and Atmospheric Physics, 51, 147-164, 1993.

560 Serreze, M. C.: Climatological aspects of cyclone development and decay in the Arctic, Journal of Atmosphere, 33, 1-23,
  1994.

Serreze, M. C., Carse, F., Barry, R. G., and Rogers, J. C.: Icelandic low cyclone activity: Climatological features, linkages
  with the NAG, and relationships with recent changes in the Northern Hemisphere circulation, Journal of Climate,
  10, 453-464, Doi 10.1175/1520-0442(1997)010<0453:Ilcacf>2.0.Co;2, 1997.

565 Serreze, M. C., and Barry, R. G.: Processes and impacts of Arctic amplification: A research synthesis, Global planetary
  change, 77, 85-96, 2011.

Singh, H. K., Bitz, C. M., Donohoe, A., and Rasch, P.: A source–receptor perspective on the polar hydrologic cycle: Sources,
  seasonality, and Arctic–Antarctic parity in the hydrologic cycle response to CO2 doubling, Journal of Climate, 30,
  9999-10017, 2017.

570 Stramler, K., Genio, A., and Rossow, W. B.: Synoptically Driven Arctic Winter States, Journal of Climate, 24, 1747-1762,
  2011.

Stroeve, J., Barrett, A., Serreze, M., and Schweiger, A.: Using records from submarine, aircraft and satellites to evaluate
  climate model simulations of Arctic sea ice thickness, The Cryosphere, 8, 1839-1854, 2014.

Thorndike, A., and Colony, R.: Sea ice motion in response to geostrophic winds, Journal of Geophysical Research: Oceans,
575  87, 5845-5852, 1982.

Tschudi, M., Stroeve, J., and Stewart, J.: Relating the age of Arctic sea ice to its thickness, as measured during NASA's
  ICESat and IceBridge campaigns, Remote Sensing, 8, 457, 2016.

Tschudi, M., Meier, W. N., Stewart, J. S., Fowler, C., and Maslanik., J.: Polar Pathfinder Daily 25 km EASE-Grid Sea Ice
  Motion Vectors, Version 4. Boulder, Colorado USA. NASA National Snow and Ice Data Center Distributed Active
580  Archive Center. doi: https://doi.org/10.5067/INAWUWO7QH7B, 2019.

Vázquez, M., Nieto, R., Drumond, A., and Gimeno, L.: Moisture transport into the Arctic: Source-receptor relationships and
  the roles of atmospheric circulation and evaporation, Journal of Geophysical Research: Atmospheres, 121,
  13,493-413,509, 2016.

Vázquez, M., Nieto, R., Drumond, A., and Gimeno, L.: Extreme Sea Ice Loss over the Arctic: An Analysis Based on
585  Anomalous Moisture Transport, Atmosphere, 8, 10.3390/atmos8020032, 2017.

Vihma, T., Tisler, P., and Uotila, P.: Atmospheric forcing on the drift of Arctic sea ice in 1989–2009, Geophysical Research
  Letters, 39, 2012.

Vihma, T., Screen, J., Tjernström, M., Newton, B., Zhang, X., Popova, V., Deser, C., Holland, M., and Prowse, T.: The
  atmospheric role in the Arctic water cycle: A review on processes, past and future changes, and their impacts,

590   Journal of Geophysical Research: Biogeosciences
121, 586-620, 2016.

Villamil-Otero, G. A., Zhang, J., He, J., and Zhang, X.: Role of extratropical cyclones in the recently observed increase in poleward moisture transport into the Arctic Ocean, Advances in Atmospheric Sciences, 35, 85-94, 2018.

Wang, X., Key, J., Kwok, R., and Zhang, J.: Comparison of Arctic sea ice thickness from satellites, aircraft, and PIOMAS
595   data, Remote Sensing, 8, 713, 2016.

Wang, X. L., Swail, V. R., and Zwiers, F. W.: Climatology and changes of extratropical cyclone activity: Comparison of ERA-40 with NCEP–NCAR reanalysis for 1958–2001, Journal of Climate, 19, 3145-3166, 2006.

Wang, X. L., Feng, Y., Compo, G., Swail, V., Zwiers, F., Allan, R., and Sardeshmukh, P.: Trends and low frequency variability of extra-tropical cyclone activity in the ensemble of twentieth century reanalysis, Climate Dynamics, 40,
600   2775-2800, 2013.

Wang, Y., Bi, H., Huang, H., Liu, Y., Liu, Y., Liang, X., Fu, M., and Zhang, Z.: Satellite-observed trends in the Arctic sea ice concentration for the period 1979–2016, Journal of Oceanology & Limnology, 037, P.18-37, 2019.

Wernli, H., and Papritz, L.: Role of polar anticyclones and mid-latitude cyclones for Arctic summertime sea-ice melting, Nature Geoscience, 11, 108-113, 2018.

605   Woods, C., and Caballero, R.: The role of moist intrusions in winter Arctic warming and sea ice decline, Journal of Climate, 29, 4473-4485, 2016.

Wu, B. Y., Wang, J., and Walsh, J. E.: Dipole anomaly in the winter Arctic atmosphere and its association with sea ice motion, Journal of Climate, 19, 210-225, Doi 10.1175/Jcli3619.1, 2006.

Yin, J. H.: A consistent poleward shift of the storm tracks in simulations of 21st century climate, Geophysical Research
610   Letters, 32, n/a-n/a, Artn L18701
10.1029/2005gl023684, 2005.

Zhang, J., and Rothrock, D.: Modeling global sea ice with a thickness and enthalpy distribution model in generalized curvilinear coordinates, Monthly Weather Review, 131, 845-861, 2003.

Zhang, J., Lindsay, R., Schweiger, A., and Steele, M.: The impact of an intense summer cyclone on 2012 Arctic sea ice
615   retreat, Geophysical Research Letters, 40, 720-726, 10.1002/grl.50190, 2013a.

Zhang, X., Walsh, J. E., Zhang, J., Bhatt, U. S., and Ikeda, M.: Climatology and interannual variability of arctic cyclone activity: 1948-2002, Journal of Climate, 17, 2300-2317, Doi 10.1175/1520-0442(2004)017<2300:Caivoa>2.0.Co;2, 2004.

Zhang, X., He, J., Zhang, J., Polyakov, I., Gerdes, R., Inoue, J., and Wu, P.: Enhanced poleward moisture transport and
620   amplified northern high-latitude wetting trend, Nature Climate Change, 3, 47-51, 2013b.